

A Cost-Sensitive Visual Question-Answer Framework for Mining a Deep And-OR Object Semantics from Web Images

Quanshi Zhang, Ying Nian Wu, and Song-Chun Zhu
University of California, Los Angeles

Abstract

This paper presents a cost-sensitive Question-Answering (QA) framework for learning a nine-layer And-Or graph (AoG) from web images, which explicitly represents object categories, poses, parts, and detailed structures within the parts in a compositional hierarchy. The QA framework is designed to minimize an overall risk, which trades off the loss and query costs. The loss is defined for nodes in all layers of the AoG, including the generative loss (measuring the likelihood for the images) and the discriminative loss (measuring the fitness to human answers). The cost comprises both human labor of answering questions and the computational cost of model learning. The cost-sensitive QA framework iteratively selects different storylines of questions to update different nodes in the AoG. Experiments showed that our method required much less human supervision (e.g. labeling parts on 3–10 training objects for each category) and achieved better performance than baseline methods.

1. Introduction

1.1. Motivation & objective

Image understanding is one of the core problems in the field of computer vision, and most previous studies implemented this task by tagging the contents inside an image, *i.e.* drawing bounding boxes of objects, segmenting image regions of “stuff” classes (*e.g.* sky, ground, and water) and classifying scene attributes (*e.g.* classroom, urban environment, and wild). However, we transfer our focus from “what is where” to the detailed statuses of each object, *i.e.* mining the semantic hierarchy of object compositions and exploring how these compositions/sub-compositions are organized in each object. Such knowledge is a prerequisite for high-level human-computer dialogue and/or interactions in the future.

Therefore, in this paper, we aim to mine deep structures of objects from web images. More importantly, we present a cost-sensitive Question-Answering (QA) framework to learn the deep structure from a very *limited num-*

ber of part annotations. Compared to previous studies, our method has the following three characteristics.

Deep and transparent representation of object compositions: In fact, obtaining a *transparent representation of the semantic hierarchy* is equivalent to *understanding detailed object statuses*, to some extent. Based on such a hierarchical representation, parsing an entire object into different semantic parts and aligning different sub-components within each part can provide rich information in object status, such as the global pose and local deformation of each certain part.

Thus, as shown in Fig. 1, a nine-layer And-Or graph (AoG) is proposed to represent visual concepts at different layers that range from *categories, poses, parts, to shape primitives* with clear semantic meanings. In the AoG, an AND node represents sub-region compositions of a visual concept, and an OR node lists a number of alternative appearance patterns of the same concept. Unlike modeling visual contexts and taxonomic relationships at the *object* level in previous studies, the AoG focuses on semantic object components and their spatial relationships.

Multiple-shot QA learning from big data: In order to scale up the technique to big data, we apply the following two strategies to limit the annotation cost. First, we collect web images using search engines as training samples without annotating object boxes. Second, as shown in Fig. 1, we design a QA framework to let the computer automatically figure out a limited number of typical examples of “*known unknowns*” in the unannotated images, ask users questions, and use the answers to refine the AoG.

Thus, as shown in Fig. 4, we design six types of questions. Each question is oriented to a certain node in the AoG, *e.g.* whether an image contains an object of a certain category and whether the current AoG provides a correct localization of an object (or a certain semantic part of a category). The computer uses these questions to overcome image noises caused by incorrect search results, intra-class variations, and ubiquitous occlusions.

Note that this multiple-shot QA learning does not fall in a conventional paradigm of active learning. First, we do not pre-define a certain feature space of an object as the prereq-

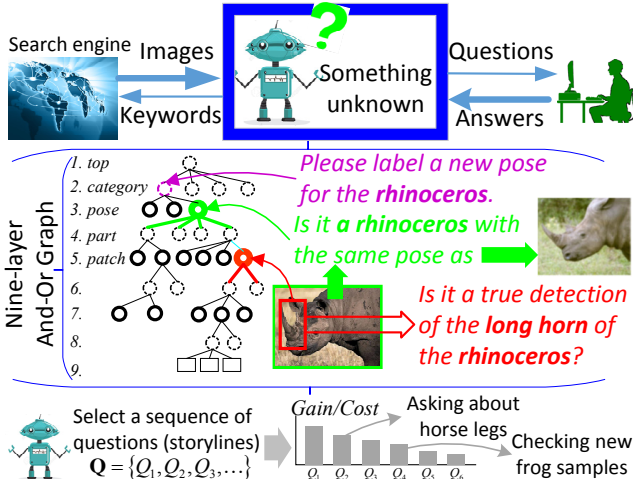


Figure 1. Question-Answer (QA) framework. The QA framework automatically collects web images from the internet, selects something unknown to ask human beings, and uses the answer to learn an And-Or graph (AoG). The AoG represents deformable structures and compositional relationships between semantic visual concepts using a 9-layer hierarchy (see Fig. 2). We formulate the generative loss and discriminative loss for the AoG, and design different questions (see Fig. 4). Each question is used to refine a certain node in the AoG. The QA framework trades off the cost and potential gain (loss decrease) of each question, and selects the best sequence of questions.

uisite of active learning. Instead, we use the QA process to gradually enrich the knowledge of object structure, *i.e.* discovering new alternative part appearance and mining the detailed components of each part. Second, we do not simply treat each answer as a single annotation of a specific object/part sample, but we generalize specific answers by mining the corresponding common patterns from big data in a weakly-supervised manner.

Cost-sensitive policy: We formulate a mixed loss for each node in the AoG as the unified paradigm to guide the learning of hierarchical object details. It includes a generative loss (measuring the model error in explaining the images) and a discriminative loss (*i.e.* the model’s fitness to human answers). Thus, among the six types of questions, each question corresponds to a certain node in the AoG, and we can use its answers to explicitly optimize the generative and/or discriminative loss of this node. Clear losses and semantic meanings of middle-layer nodes make our deep AoG different from deep neural networks.

As shown in Fig. 1, the QA framework uses the node loss to identify the nodes that are insufficiently trained, and selects the best sequence of questions to optimize a list of AoG nodes in an online manner. In each step, the QA framework balances the costs and potential gains of different questions, and selects the questions with high gains and low costs, to ensure high learning efficiency, which trades

off the generative and discriminative losses, the human labor for annotations, and the computational cost.

In fact, this cost-sensitive policy is extensible. In this study, the QA framework combines six types of questions and four modules of 1) graph mining [44] (unsupervised mining of AoG structures without the labeling of object locations), 2) And-Or template learning [35] (discovery of detailed structures within aligned parts), 3) supervised learning, and 4) object parsing. In addition, people can extend the QA system by adding more questions and modules.

1.2. Related work

Knowledge organization for big data: Many studies organized models of different categories in a single system. The CNN [27] encodes knowledge of thousands of categories in numerous neurons. It is difficult to identify clear semantic meanings and their relationships in most neurons.

Recently, there has been a growing interest in modeling high-level knowledge beyond object detection. [8, 9] mined models for different categories/subcategories from web images. [13] constructed a hierarchical taxonomic relationships between categories. [48, 25, 39, 3] formulated the relationships between natural language and visual concepts. [1] further built a Turing test system. [16] modeled the contextual knowledge between objects. Knowledge in these studies was mainly defined upon object-level models (*e.g.* the affordance and context). In contrast, we explore deep structures within objects. The deep hierarchy of parts provides a more informative understanding of object statuses.

Multiple-shot QA for learning: Many weakly-supervised methods and unsupervised methods have been developed to learn object-level models. For example, studies of [6, 38, 31, 15, 44], object co-segmentation [23], and object discovery [36, 43] learned with image-level annotations (without object bounding boxes). [11, 45] did not require any annotations during the learning process.

However, when we explore detailed object structures, manual annotations are still necessary to avoid model drift. Therefore, inspired by active learning methods [40, 42, 20, 30, 26], we hope to use a very limited number of human-computer QAs to learn each object pose. In fact, such QA ideas have been applied to object-level models [14, 33, 41]. Branson *et al.* [4] used human-computer interactions to point out locations of object parts to learn part models, but they did not provide part boxes. In contrast, we focus on deep object structures. we design six types of human-computer dialogues/QAs for annotations (see Fig. 4). Our QA system chooses questions based on the generative and discriminative losses of AoG nodes, thereby explicitly refining different AoG nodes. In experiments, our method achieved good performance when we only label parts on 3–5 objects for each pose.

Transparent representation of structures is closely re-

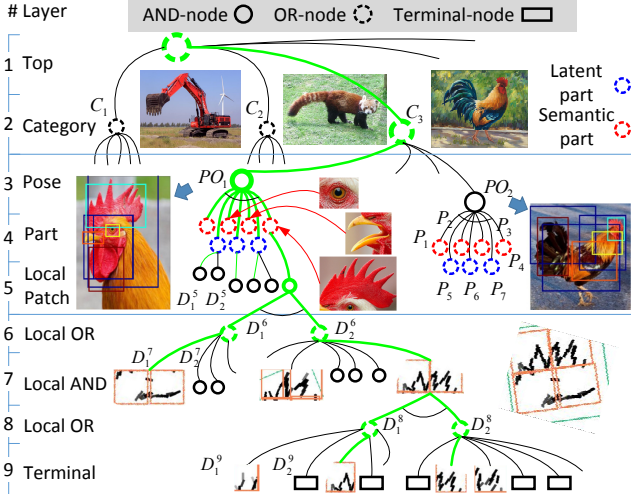


Figure 2. A nine-layer And-Or Graph. An object can be explained by a *parse graph* $\hat{p}g$, which is indicated by green lines. In the parse graph, AND nodes encode deformable structures between local patches, and OR nodes contain alternative local patterns. Each *pose* has both *latent parts* without names (blue OR nodes \rightarrow blue rectangles on roosters) and *semantic parts* with specific names (red OR nodes \rightarrow other rectangles on roosters).

lated to deep understanding of object statuses. Beyond the object bounding box, we can further parse the object and align visual concepts at different layers to different object parts/sub-parts, which provides rich information of local appearance and poses. In previous studies, part models were mainly designed with single-layer latent parts [36, 17] or single-layer semantic parts [2, 7, 32, 46, 22, 4], and trained for object detection with strong supervision. Whereas, we have a different objective, *i.e.* weakly-supervised mining the deep structural hierarchy of objects.

1.3. Contributions

The paper makes the following contributions:

- 1) To the best of our knowledge, we are the first to learn a deep semantic hierarchy of objects, which is so deep as a nine-layer AoG.
- 2) We propose an efficient QA framework that allows the computer to discover something unknown, to ask questions, and to explicitly learn deep object structures from human-computer dialogues.
- 3) We use a general and extensible cost-sensitive policy to implement the QA system, which ensures a high efficiency of mining knowledge. To the best of our knowledge, our method is the first to reduce the cost of learning part localization to about 10 annotations for each part.
- 4) Our QA framework is not oriented to certain datasets with limited samples, but an open system that is suitable for big data and human-computer dialogues.

2. Representation with the And-Or graph

Fig. 2 shows the nine-layer AoG, which encodes visual concepts at different levels within objects and organizes their hierarchy. The basic element of the AoG is the three-layer And-Or structure in Fig. 3, where an AND node represents 1) part compositions of a certain concept and 2) their deformation information, and an OR node lists alternative local patterns for a certain part. Let θ denote all the AoG parameters. Let us use the AoG for object parsing in image I . For each node D in the AoG, we use Λ_D and $\theta_D \subset \theta$ to denote the image region corresponding to D and the parameters related to D , respectively.

Each Terminal node T in the bottom layer represents a pattern of local shape primitives. The reference score of node T in image I is formulated as

$$S_I(T) = \langle \omega_T, \Phi(I_{\Lambda_T}) \rangle \quad (1)$$

where $\Phi(I_{\Lambda_T})$ denotes the local features for the region Λ_T in I , and $\theta_T = \omega_T$ is the parameter.

Each OR node O in the AoG provides a list of alternative local appearance patterns. In particular, OR nodes in Layers 1 and 2 encode the category choices and possible object poses within each category, respectively, and those in Layers 4, 6, and 8 offer local pattern candidates. When we use the AoG for object inference in image I , O selects its child node with the highest score as the true configuration:

$$S_I(O) = \max_{D \in Ch(O)} S_I(D) \quad (2)$$

where function $Ch(\cdot)$ indicates the children set of a node. The child node D can be a Terminal node, an OR node, or an AND node. Note that “invisible” $\in Ch(O)$ is also a child of O , which is activated when other children patterns cannot be detected.

Each AND node A in the AoG contains a number of sub-region components, and it models their geometric relationships. In particular, the AND nodes in Layer 3 organize the relationship between object *poses* and object *parts*, and those in Layers 5 and 7 encode detailed structural deformation within part patches. The inference score of A is formulated as the sum of its children’s scores:

$$S_I(A) = w_A \left[S_I^{app}(A) + \sum_{D \in Ch(A)} S_I(D) + \sum_{(D, D') \in \mathcal{N}(A)} w_{DD'} S_I(D, D') \right] + b_A \quad (3)$$

where $S_I^{app}(A)$ represents the score of the global appearance in the region Λ_A . $\mathcal{N}(A)$ denotes the set of A ’s neighboring children pairs. $S_I(D, D')$ measures the deformation between image regions Λ_D and $\Lambda_{D'}$ of sibling children D and D' . $w_{DD'}$ and $w_A, b_A \in \theta_A$ are weighting parameters for normalization.

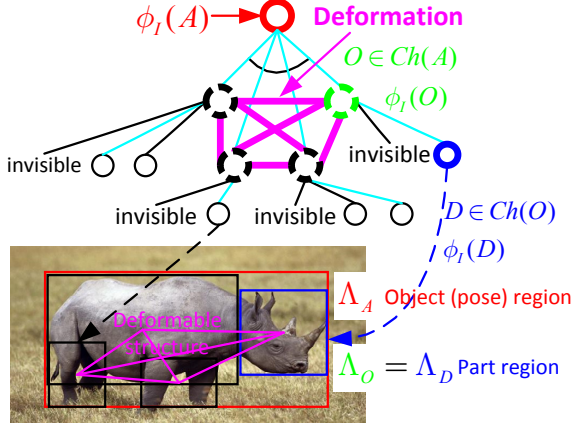


Figure 3. Three-layer And-Or/And/Terminal structure in the AoG. Cyan lines indicate a parse graph for object inference.

2.1. Design of Layers 3–5

Layers 3 → 4: The three-layer And-Or structure that ranges across the *pose*, *part*, and *local* layers is derived from the AoG pattern proposed in [44]. This technique models the three-layer sub-AoG as the common subgraph pattern that frequently appears among a number of large graphs (*i.e.* images). For each *pose* node PO under a category node C , we do not model its global appearance. PO contains two types of children nodes, *i.e.* *latent* children (the parts mined automatically from big data without clear semantic meaning) and *semantic* children (the parts with certain names).

Part deformation: We connect all pairs of *part* nodes under pose PO as neighbors. For each pair of *part* nodes $(P, P') \in \mathcal{N}(PO)$, the deformation score between them measures the squared difference between the ideal (average) geometric relationship $\Phi(P, P')$ and the actual part relationship detected in the image $\Phi(\Lambda_P, \Lambda_{P'})$. In addition, we also assign a specific deformation penalty ρ as the deformation score, when one of the parts are not detected. In [44], the average geometric relationship $\Phi(P, P')$ and the penalty is estimated.

Layers 4 → 5: To simplify the AoG, we allow latent part nodes to have multiple children, but the semantic part node can only have one child besides the “invisible” child. For each child D in Layer 5 of a *latent part*, its appearance score measures the squared difference between D ’s ideal (average) appearance $\Phi(D)$ and the actual appearance detected in the image $\Phi(I_{\Lambda_D})$. Then, for the only child D' of an *semantic part*, we use part annotations to train a linear SVM to classify its local appearance, and set the appearance score of D' as the SVM score. We also assign a specific appearance penalty for “invisible” children in Layer 5. Finally, we use the pose model for object inference in background images, and normalize the overall pose score with zero mean and unit variation. Model parameters, including average part appearance $\Phi(D)$, the SVM parameters for semantic parts,

the appearance penalty, and the normalization parameters, would be learned in [44].

Features: As in [44], appearance features for each patch D in Layer 5 comprise the HOG features and the height-width ratio of the patch. Three types of pairwise features are used to describe geometric relationships between *parts* P and P' in Layer 4, including 1) $\log(\frac{s_P}{s_{P'}})$, 2) $\frac{p_P - p_{P'}}{\|p_P - p_{P'}\|}$, and 3) $\log \frac{\|s_P, s_{P'}\|}{\|p_P - p_{P'}\|}$, where s_P and p_P denote the scale and 2D position of the part P , respectively.

2.2. Design of Layers 5–9

The bottom four layers (Layers 6–9) of the AoG represent detailed structures within the *semantic patches* in Layer 5 based on the And-Or template proposed in [35]. First, for each AND node A in Layers 5 and 7, we do not encode its global appearance. A has two children, and the deformation relationship between the two children is used to roughly model the “*geometric OR* relationships” involved in [35]. Second, each OR node O in Layers 6 and 8 has a number of children, which encodes only the “*structural OR* information” described in [35]. Finally, terminal nodes in Layer 9 are described by the HIT feature mined by [34], which combines information of sketches, texture, flat area, and colors of a local patch.

2.3. Object parsing (inference)

Given an image I , we use the AoG to perform hierarchical parsing for the object inside I , *i.e.* estimating a *parse graph* (see green lines in Figs.2) to explain the object:

$$\hat{p}g = \operatorname{argmax}_{pg} S_I(pg) \quad (4)$$

where we define the parse graph as a set of activated node regions for object understanding, $\hat{p}g = \{\Lambda_{\hat{C}}, \Lambda_{\hat{F}O}, \hat{\Lambda}_{P_1}, \hat{\Lambda}_{P_2}, \dots, \hat{\Lambda}_{D_1^g}, \dots, \hat{\Lambda}_{D_n^g}\}$, which describes an inference tree of the AoG. We can understand the parse graph in a top-down manner. 1) Let an OR node O in Layers 1, 2, 4, 6, or 8 have been activated and put into the parse graph ($\hat{\Lambda}_O \in \hat{p}g$). O activates its best child $\hat{D} = \operatorname{argmax}_{D \in Ch(O)} S_I(D)$ to explain the O ’s image region $\Lambda_{\hat{D}} = \hat{\Lambda}_O$, and puts \hat{D} into the parse graph ($\Lambda_{\hat{D}} \in \hat{p}g$). 2) Let an AND node \hat{A} in Layers 3, 5, or 7 have been activated and put into the parse graph ($\Lambda_{\hat{A}} \in \hat{p}g$). \hat{A} determines the best image region inside $\Lambda_{\hat{A}}$ for each of its OR children $O \in Ch(\hat{A})$, *i.e.* $\{\hat{\Lambda}_O\} = \operatorname{argmax}_{\{\Lambda_O\}} S_I(A)|_{\{\Lambda_O\}}$, and put $\{\hat{\Lambda}_O\}$ into the parse graph. Therefore, because we do not encode the global appearance of pose nodes, the objective of object

parsing can be rewritten as

$$\begin{aligned} \max_{pg} S_I(pg) &= \max_{PO \in \Omega_{pose}} S_I(PO) \\ &= \max_{PO \in \Omega_{pose}} \max_{\{\Lambda_P\}} w_{PO} \left\{ \sum_{P \in Ch(PO)} S_I(P) \right. \\ &\quad \left. + \sum_{(P, P') \in \mathcal{N}(PO)} w_{PP'} S_I(P, P') + b_{PO} \right\} \end{aligned} \quad (5)$$

where Ω_{pose} is the set of pose nodes in the AoG. The target parse graph pg for Layers 3–5 can be estimated via graph matching [44]. As mentioned in [44], (3) is a typical quadratic assignment problem that can be directly solved by optimizing a Markov random field [24]. The detailed inference for Layers 6–9 is solved by using [35]. The left-right symmetry of objects is considered in applications.

3. Cost-sensitive Question-Answer learning

3.1. Brief overview of QA-based learning

In this section, we define the overall risk of the AoG. We use this risk to guide the growth of the AoG, which includes the selection of the questions, refining the current visual concepts in the AoG based on the answers, and mining new concepts as new AoG branches. The overall risk combines both the cost of asking questions during the learning process and the loss of AoG representation. The loss of AoG representation further comprises the generative loss (*i.e.* the fitness between the AoG and real images) and the discriminative loss (*i.e.* the AoG fitness to human supervision).

Therefore, the minimization of the AoG risk is actually to select a limited number of questions that can potentially minimize the AoG loss. In fact, we organize the six types of questions into four types of QA storylines (Fig. 4). In each step of the QA process, we conduct a certain storyline to decrease the risk. Meanwhile, we evaluate the gain (loss decrease) of different AoG nodes after each storyline, so that we can determine the next best storyline in an online manner.

Unlike previous active learning methods that directly use human annotations as ground-truth samples for training, we generalize specific annotations to common patterns among big data so as to update the AoG.

For example, in Layer 4 of the AoG, there are two types of parts, *i.e.* the *semantic parts* and *latent parts*. In Storylines 3 and 4 (details will be discussed later), we first 1) ask for a number of object samples with a certain pose, 2) based on the object examples, select a large number of similar objects from all the web images as potential positives of this pose, then 3) mine the common part patterns among these objects as the *latent parts*, and 4) model their spatial relationships.

Thus, as in (3) and Fig. 3, spatial relationships between latent parts constitute a graph that represents the latent

structure of the pose. Then, we continue to ask for semantic parts in Storylines 3 and 4, and use the pre-mined latent pose structure to localize relative positions of the newly annotated semantic parts. Such a combination of structure mining from big data and part annotations on small data ensures a high learning stability.

In the following subsections, we introduce the detailed implementations of the proposed QA framework.

3.2. Notation

As shown in Fig. 4, we design six types of questions to learn the AoG, and organize these questions into four types of storylines. Let us assume that the QA framework has selected a sequence of storylines $\mathbf{Q} = \{Q_1, Q_2, \dots\}$, and modified the AoG parameters to $\hat{\theta}(\mathbf{Q})$. We use the system risk, $Risk(\mathbf{Q})$, to evaluate the overall quality of the current status of QA-based learning. The objective of the QA framework is to select the storylines \mathbf{Q} that can greatest decrease the overall risk:

$$\begin{aligned} \hat{\mathbf{Q}} &= \operatorname{argmin}_{\mathbf{Q}} Risk(\mathbf{Q}) \\ Risk(\mathbf{Q}) &= \mathbf{L}(\hat{\theta}(\mathbf{Q})) + Cost(\mathbf{Q}) \end{aligned} \quad (6)$$

The system risk comprises the cost of the storylines $Cost(\mathbf{Q})$ and the loss (inaccuracy) of the current AoG $\mathbf{L}(\hat{\theta}(\mathbf{Q}))$. Thus, we can expect the QA system to select *cheap* storylines $\hat{\mathbf{Q}}$ that greatly improve the model quality.

Definition of \mathbf{Q} and its cost: Let Ω denote the set of storylines. In fact, the QA system selects a sequence of storylines $\mathbf{Q} = \{Q_i \in \Omega\}_{i=1,2,\dots}$ to modify the AoG. Each storyline line $Q_i \in \Omega$ comprises a number of questions and learning modules. As shown in Table 1, we can represent the storyline as a three-tuple $Q_i = (M_i, U_i, PO_i)$. Q_i proposes some questions $M_i \subset \{q_1, q_2, \dots, q_6\}$ (q_j is a question defined in Fig. 4) for the target parse graph of the pose PO_i , expects a tutor U_i to answer these questions, and then uses the answers for training. These storylines choose ordinary users, professional instructors, or the computer itself as the tutor U_i to answer these queries.

In addition, each storyline Q_i has a certain cost $Cost(Q_i)$ according to both human labor of answering and the computational cost of model learning¹. The overall cost of \mathbf{Q} is given as

$$Cost(\mathbf{Q}) = \sum_i Cost(Q_i) \quad (7)$$

Definition of the AoG loss: Let $\mathbf{I} = \{I_1, I_2, \dots\}$ be a comprehensive web image dataset governed by the underlying distribution $f(I)$. When we use our AoG (with parameters $\hat{\theta}$) to explain the images in \mathbf{I} , we can formulate the

¹Professional instructors have higher labor cost considering their professional levels.

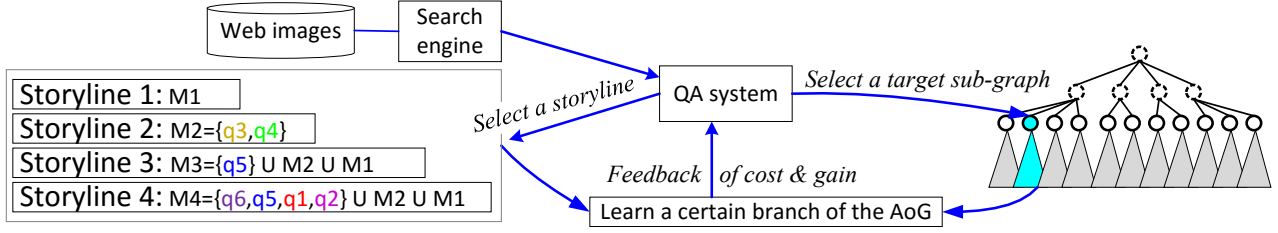
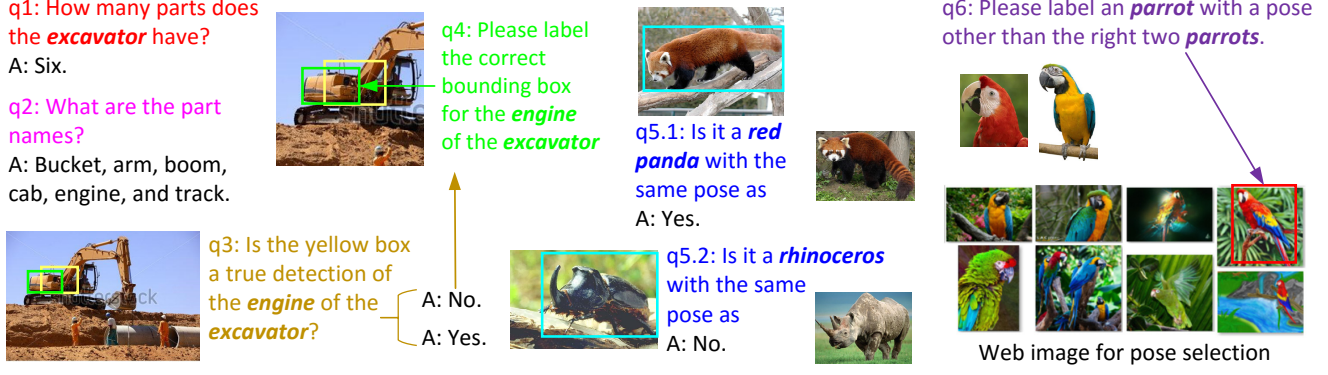


Figure 4. Design of questions (top) and the QA framework (bottom). The QA framework iteratively selects a storyline and applies it to a target sub-AoG.

overall loss as

$$L(\hat{\theta}) = E_{I \sim f(I)} \left[\underbrace{-S_I(pg^*)}_{\text{generative loss}} + \underbrace{L(pg^*, \hat{p}g(\hat{\theta}))}_{\text{discriminative loss}} \right] \quad (8)$$

where pg^* and $\hat{p}g$ indicate the true parse graph configuration and the estimated configuration of I , respectively. The generative loss measures the fitness between the image I and its true parse graph pg^* , and the discriminative loss evaluates the classification performance.

The generative loss can be rewritten as

$$E_f[-S_I(pg^*)] = \sum_{PO} P(PO) L_{PO}^{gen}, \quad (9)$$

$$L_{PO}^{gen} = E_{I \in \mathbf{I}_{PO}} [-S_I(PO)]$$

where $\mathbf{I}_{PO} \subset \mathbf{I}$ represents a subset of images that contain objects belonging to the pose PO , and L_{PO}^{gen} denotes the average generative loss of images in \mathbf{I}_{PO} . $\Lambda_{PO} \in pg^*$ indicates the true pose of the object inside I . $P(PO) = |\mathbf{I}_{PO}|/|\mathbf{I}|$ measures the probability of PO .

The discriminative loss for the pose PO comprises the loss for category (pose) classification L_{PO}^{cate} and the loss for part localization L_{PO}^{part} :

$$E_f[L(pg^*, \hat{p}g(\hat{\theta}))] = \sum_{PO} P(PO) \{L_{PO}^{cate} + L_{PO}^{part}\} \quad (10)$$

where $L_{PO}^{cate} = V^{cate} E_{I \in \mathbf{I}_{PO}} \{ \max\{0, \Delta(\hat{C}, C^*) + [S_I(\hat{C}) - S_I(C^*)] \} \}$, $L_{PO}^{part} = V^{part} E_{I \in \mathbf{I}_{PO}, P \in Ch(PO)} \{ \max\{0, \Delta(\hat{\Lambda}_P, \Lambda_P^*) + [S_I(P)|_{\hat{\Lambda}_P} - S_I(P)|_{\Lambda_P^*}] \} \}$. $\Lambda_{\hat{C}}, \hat{\Lambda}_P \in \hat{p}g$, $\Lambda_{C^*}, \Lambda_P^* \in pg^*$. V^{cate} and V^{part} represent prior weights for category classification and part localization, respectively (here, we set $V^{cate} = 1.0$, $V^{part} = 1.0$).

3.3. Learning procedure

In the beginning, we use K keywords to crawl web images of K categories from the internet, and build a comprehensive web image dataset $\mathbf{I} = \{I_1, I_2, \dots\}$. Next, we apply Storyline 4 to each category, which mines an initial model for a certain pose of this category. Then, we simply use a greedy strategy to solve (6), which estimates a sequence of storylines $\mathbf{Q} = \{Q_i\}_{i=1,2,\dots}$. In each step i , we recursively determine the next best storyline, \hat{Q}_i , as follows.

$$\hat{Q}_i = \operatorname{argmax}_{Q_i \in \Omega} \frac{-\Delta L(\hat{\theta}(\mathbf{Q}))}{Cost(Q_i)} \quad (11)$$

where $\Delta L(\hat{\theta}(\mathbf{Q}))$ denotes the potential AoG gain (decrease of the AoG loss, which is estimated by historical operations and introduced later) from storyline \mathbf{Q} . Considering (9) and (10), we can rewrite the above equation as

$$\hat{Q}_i = \operatorname{argmax}_{Q_i = (M_i, U_i, PO_i)} \frac{-P(PO_i) [\Delta L_{PO_i}^{gen} + \Delta L_{PO_i}^{cate} + \Delta L_{PO_i}^{part}]}{Cost(Q_i)} \quad (12)$$

where $\Delta L_{PO_i}^{gen}$, $\Delta L_{PO_i}^{cate}$, and $\Delta L_{PO_i}^{part}$ are the potential gains of $L_{PO_i}^{gen}$, $L_{PO_i}^{cate}$, and $L_{PO_i}^{part}$ after storyline \hat{Q}_i , respectively. $P(PO_i)$ can be estimated based on the current web images collected for PO_i (i.e. $\hat{\mathbf{I}}_{PO_i}$)² and the yes/no answer ratio during sample collection in Storyline 3.

² $\hat{\mathbf{I}}_{PO_i}$ denotes the current images that are collected for pose PO_i from a category's image pool \mathbf{I}_C in Storyline 3.

Table 1. Four types of storylines for each pose PO_i .

| # | Question stories M_i for pose PO_i | Participants U_i | $\Delta L_{PO_i}^{gen}$ | $\Delta L_{PO_i}^{cate}$ | $\Delta L_{PO_i}^{part}$ | $Cost(Q_i)$ |
|---|---|---------------------------|-------------------------|--------------------------|--------------------------|--|
| 1 | retrain category classification | Computer | | ✓ | | $C_{PO_i}^{ret}$ |
| 2 | check & correct inaccurate semantic part localizations | Users | | ✓ | ✓ | $C_{PO_i}^{ckp} + C_{PO_i}^{lbp}$ |
| 3 | 1) QA-based collection of object samples for pose PO_i , 2) mine the latent structure of pose PO_i | Users & Computer | ✓ | ✓ | ✓ | $C_{PO_i}^{col} + C_{PO_i}^{cko} + C_{PO_i}^{ckp}$ $+ C_{PO_i}^{lbp} + C_{PO_i}^{ret}$ |
| 4 | generate a new pose: label an initial object example, collect samples, mine latent structure, label parts | Instructors & Computer | ✓ | | | $C_{PO_i}^{pose} + 3C_{PO_i}^{col} + 3C_{PO_i}^{cko}$ $+ C_{PO_i}^{lbp} + C_{PO_i}^{ret}$ |

3.4. Introduction of storylines

Storyline 1: retraining category classification. As the QA framework collects more and more web images, in this storyline, we use these images to update the AoG parameters for the classification of a certain pose PO_i . This storyline mainly decreases the discriminative loss $L_{PO_i}^{cate}$.

Given all the web images that have been collected for pose PO_i (*i.e.* $\hat{\mathbf{I}}_{PO_i}$ ²) we use the current AoG for object inference on these images. Given an incorrect object inference (*i.e.* an image is incorrectly recognized as a pose PO_j other than the true pose PO_i), we can use this inference result to produce hard negatives of semantic object parts for PO_j , and retrain its part classifier in Layer 5.

Therefore, the potential cost for a future storyline $Cost(Q_i)$ mainly comprises the computational cost of object inference $C_{PO_i}^{ret} = \lambda^{ret} |\hat{\mathbf{I}}_{PO_i} || \Theta_{pose} |$, where Θ_{pose} is the set of all the pose nodes, and λ^{ret} is a weighting parameter³. The potential gain $\Delta L_{PO_i}^{cate}$ can be predicted simply using historical gains from similar storylines for pose PO_i ⁴.

Storyline 2: checking & labeling semantic parts. In this storyline, the computer 1) selects a sequence of images, 2) asks users whether the current AoG can correctly localize the semantic parts in these images, and 3) lets users correct the incorrect part localizations to update the AoG.

First, the QA system uses the pose model of PO_i for object inference on the images $\hat{\mathbf{I}}_{PO_i} \subset \hat{\mathbf{I}}_{PO_i}^{unlabeled}$ in which semantic parts are not labeled. Next, the QA system selects a set of images that potentially contain incorrect localizations of semantic parts. We select the object samples that have good localizations of latent parts but inaccurate localizations of semantic parts, *i.e.* having high scores for latent parts but low scores for semantic parts. Thus, we can determine the target sample (image) as $\hat{I} = \operatorname{argmax}_{I \in \hat{\mathbf{I}}_{PO_i}^{unlabeled}} S_I(PO_i) - S_I(PO_i^{lat})$, where PO_i^{lat} is a dummy pose that is constructed by eliminating semantic parts from the current pose.

³Please see Section 4.1 for parameter settings of λ^{x} .

⁴Among all the storylines Q_j , $j = 1, \dots, i-1$ before Q_i , we select the storylines that have both the same type of questions $M_j = M_i$ and the same target pose $PO_j = PO_i$ as Q_i . We record gains of $\Delta L_{PO_i}^{cate}$ and $\Delta L_{PO_i}^{part}$ after these storylines, and use these historical gains to predict the gain for a further storyline pi_i .

Then, the computer asks users to check whether the part localizations on the selected images are correct or not⁵ (see Fig. 4(q_3)), and finally asks users to label the boxes for the incorrect part localizations (see Fig. 4(q_4)).

Given the annotations of semantic part boxes, we update the geometric relationships between *part* nodes in Layer 4 based on [44], and update SVM classifiers for local patch appearance in Layer 5. Given the part annotations, we can further learn detailed structures in Layers 5–9 via [35].

The cost $Cost(Q_i)$ of this storyline mainly comprises the human labor required for both part checking $C_{PO_i}^{ckp}$ and part labeling $C_{PO_i}^{lbp}$, which can be measured as $C_{PO_i}^{ckp} = \lambda^{ckp3} |SemanticCh(PO_i)|$, and $C_{PO_i}^{lbp} = \lambda^{lbp3} |SemanticCh(PO_i)|$, respectively. This storyline mainly decreases $L_{PO_i}^{cate}$ and $L_{PO_i}^{part}$. The potential gain $\Delta L_{PO_i}^{cate}$ and $\Delta L_{PO_i}^{part}$ for a future storyline can be predicted using historical gains⁴.

Storyline 3: collecting & labeling new samples. This storyline collects new sample for pose PO_i from web images to update the pose. It decreases the generative loss $L_{PO_i}^{gen}$ and the pose classification loss $L_{PO_i}^{cate}$. First, we use the sub-AoG of pose PO_i to collect new samples from web images⁶ with top inference scores. The system collects $N = 3 \cdot 1.5^k$ new samples, when it is the k -th time to perform Storyline 3 to pose PO_i .

Second, we randomly select n ($n = 10$, here) new object samples, ask users whether they are true samples with pose PO_i , and expect yes/no answers (see Fig. 4($q_{5.1}$, $q_{5.2}$)).

Third, given the true samples, we use graph mining [44] to refine the And-Or structure in Layers 3–5 for PO_i . The sub-AoG is refined towards the common subgraph pattern (pose model) embedded in a set of large graphs (images). Its objective can be roughly written as follows, which is proved in Appendix 6.1.

$$\operatorname{argmax}_{\theta_{PO_i}} E_{I \in \hat{\mathbf{I}}_{PO_i}} [S_I(PO_i)] \exp[-\text{ModelComplexity}(\theta_{PO_i})] \quad (13)$$

The above equation refines the θ_{PO_i} by 1) adding (or delet-

⁵The QA system asks about part compositions/names for pose PO_i in the first time of part labeling (see Fig. 4(q_1 , q_2)).

⁶The images collected from search engines comprise both correct images with target objects and irrelevant background images.

ing) new (or redundant) latent parts $P \in \text{LatentCh}(PO_i)$ from the pose PO_i , 2) determine the children number (i.e. the number of patches in Layer 5) of each latent part P , 3) updating the average appearance $\Phi(D)$ of each patch $D \in \text{Ch}(P)$, and 4) refining the average geometric relationship $\Phi(P, P')$ between each pair of children parts $P, P' \in \text{Ch}(PO_i)$.

In the end of Storyline 1, we further apply Storylines 2 and 1 to refine semantic parts for pose PO_i and retrain for pose classification.

Therefore, the potential cost of a future storyline can be computed as $\text{Cost}(Q_i) = C_{PO_i}^{col} + C_{PO_i}^{cko} + C_{PO_i}^{ckp} + C_{PO_i}^{lbp} + C_{PO_i}^{ret}$. $C_{PO_i}^{col} = \lambda^{col} |\mathbf{I}_C|$ is the computational cost of sample collection, where \mathbf{I}_C denotes the entire web image pool of category C , $PO_i \in \text{Ch}(C)$. $C_{PO_i}^{cko} = \lambda^{cko} n$ indicates the human labor of checking samples. $C_{PO_i}^{ckp}$, $C_{PO_i}^{lbp}$, and $C_{PO_i}^{ret}$ denote the costs of checking parts, labeling parts, and retraining pose classification, respectively, and can be estimated as introduced in Storylines 1 and 2. This storyline mainly decreases $L_{PO_i}^{gen}$, $L_{PO_i}^{cate}$ and $L_{PO_i}^{part}$. For the term of $L_{PO_i}^{gen}$, we can roughly estimate $P(PO_i) \Delta L_{PO_i}^{cate}$ as $-\text{mean}_{\mathbf{I}_C} \Delta S_I(C)$, $PO_i \in C$ in the last Storyline 3. $\Delta L_{PO_i}^{cate}$, $\Delta L_{PO_i}^{part}$ are approximated using historical gains⁴.

Storyline 4: labeling a new sibling pose. As shown in Fig. 4(q_6), in this storyline, the QA system requires a professional instructor to label an initial sample for a new pose PO_i in category C , and uses iterative graph mining [44] to extract the structure of Layers 3–5 for pose PO_i (only mining latent parts in Layer 5). The graph mining is conducted with three iterations. In each iteration, we first collect new object samples for pose PO_i , as shown in Fig. 4($q_{5.1}$, $q_{5.2}$). Based on the collected samples, we optimize the mining objective in (13) to mine/refine the latent parts in Layer 4 and the patches in Layer 5 for this pose. In this way, we obtain the latent structure of the new pose PO_i , and then we apply Storylines 2 to pose PO_i to ask and label semantic parts and to fix these semantic parts on this latent structure. Finally, we apply Storyline 1 to train classifiers of the semantic parts for pose classification.

Therefore, the storyline cost is given as $\text{Cost}(Q_i) = C_{PO_i}^{pose} + 3C_{PO_i}^{col} + 3C_{PO_i}^{cko} + C_{PO_i}^{lbp} + C_{PO_i}^{ret}$, where $C_{PO_i}^{pose} = \lambda^{pose}$ is a constant cost for labeling a new pose³, and other costs can be estimated as mentioned above. This storyline mainly decreases $L_{PO_i}^{gen}$, which can be computed as in Storyline 3.

4. Experiments

4.1. Details

To implement the QA system, we set the parameters as follows: Considering that the time cost of labeling a part is usually five times greater than that of making a yes/no judgment, we set $\lambda^{ckp} = 1.0$, $\lambda^{cko} = 1.0$, and $\lambda^{lbp} = 5$. The computational cost of the collection/inference of each

object was set as $\lambda^{ret} = 0.01$, $\lambda^{col} = 0.01$. We set $\lambda^{pose} = 50$ as the labeling cost for a new pose.

We applied Bing Search and used 16 different keywords to collect web images. The keywords included “bulldozer,” “crab,” “excavator,” “frog,” “parrot,” “red panda,” “rhinoceros,” “rooster,” “*Tyrannosaurus rex*,” “horse,” “equestrian,” “riding motorbike,” “bus,” “aeroplane,” “fighter jet,” and “riding bicycle.” With each keyword, we collected the top-1000 returned images. We used images of the first ten keywords to learn an AoG (namely *AoG-10*) with ten categories to evaluate the learning efficiency of our QA framework. Then, we used images of the last seven keywords to learn an AoG (namely *AoG-7*) with five categories (*horse*, *motorbike*, *bus*, *aeroplane*, and *bicycle*) and tested the performance on the Pascal VOC dataset [18].

4.2. Mining of the deep semantic hierarchy

Fig. 6 illustrates the deep structures of some categories in the *AoG-10*. The QA system applied a total of 39 storylines to learn *AoG-10*. The *AoG-10* contains two poses for the *frog*, *horse*, and *parrot* categories, and three poses for each of the other seven categories in Layer 3. *AoG-10* has 132 semantic part nodes and 84 latent part nodes in Layer 4. *AoG-7* contains a total of 12 pose nodes in Layer 3, 48 semantic part nodes, and 48 latent part nodes in Layer 4.

4.3. Evaluation in terms of part localization

The objective of this work is to learn a transparent representation of deep object hierarchy, it is difficult to evaluate the quality of deep structures. Therefore, we evaluate our AoGs in terms of part localization, although our contribution is far more than it. We tested the *AoG-10* on web images and tested the *AoG-7* on the Pascal VOC dataset for a comprehensive evaluation.

Baselines: Our AoGs were learned with part annotations on only 2–14 objects in each category, but most previous methods require a large number of part annotations to produce a valid model. Nevertheless, we still selected the eight baselines for comparisons, including benchmark methods for object detection (here is part detection), popular part-localization approaches, and methods for interactive learning of parts. For each baseline, we randomly selected different number of training samples to learn the model and enable a fair comparison.

First, we focused on [2], which uses annotations of semantic parts to train DPMs. This method clusters training samples to different object poses, and trains a DPM component for each pose. We designed three baselines based on [2], namely *SSDPM-2*, *SSDPM-3* and *SSDPM-5*. For each category, *SSDPM-2*, *SSDPM-3* and *SSDPM-5* learned two, three, and five pairs of left-right symmetric poses, respec-



Figure 5. AoG-based part localization. (Left) Explanation of parts in Layer 4. (Right) Semantic parts that are detected from different objects.

Table 2. Performance of part localization

| | bicyc-L | | bicyc-R | | bus-L | | bus-R | | aero-L | | aero-R | | | | |
|----------------|------------|-------------|-------------|-------------|-------------|-------------|-------------|-------------|-------------|-------------|-------------|-------------|-------------|-------------|-------------|
| | #box | APP | AER | APP | AER | #box | APP | AER | APP | AER | #box | APP | AER | APP | AER |
| SSDPM [2] | 228 : | 58.7 | 58.4 | 67.2 | 65.7 | 98 : | 30.0 | 36.8 | 20.6 | 30.7 | 133 : | 13.9 | 22.2 | 24.6 | 31.0 |
| | 110 : | 53.2 | 55.0 | 54.7 | 58.5 | 57 : | 3.3 | 23.2 | 5.9 | 18.0 | 68 : | 7.7 | 15.4 | 12.3 | 31.8 |
| P-Graph [7] | 204 : | 8.3 | 0 | 5.4 | 0 | 152 : | 11.2 | 0 | 15.9 | 0 | 156 : | 1.7 | 0 | 1.7 | 0 |
| Fast-RCNN [21] | 222 : | 23.0 | 2.6 | 21.3 | 1.8 | 109 : | 19.0 | 0 | 20.1 | 6.7 | 95 : | 14.6 | 4.2 | 16.8 | 2.3 |
| | 113 : | 24.1 | 5.1 | 15.1 | 0 | 51 : | 3.0 | 0 | 12.6 | 6.7 | 49 : | 5.7 | 0 | 7.0 | 0 |
| Our | 9 : | 60.6 | 60.5 | 68.8 | 65.1 | 54 : | 36.7 | 35.4 | 35.3 | 41.7 | 24 : | 13.9 | 28.4 | 17.5 | 31.0 |
| | motor-L | | motor-R | | horse-L | | horse-R | | | | | | | | |
| | #box | APP | AER | APP | AER | #box | APP | AER | APP | AER | | | | | |
| SSDPM [2] | 30 : | 57.9 | 57.3 | 24.5 | 41.5 | 104 : | 10.1 | 40.6 | 9.5 | 35.5 | | | | | |
| | 24 : | 0 | 7.7 | 0 | 8.0 | 52 : | 0 | 18.7 | 1.4 | 16.2 | | | | | |
| P-Graph [7] | 148 : | 7.1 | 0 | 9.3 | 0 | 180 : | 3.7 | 0 | 0.6 | 0 | | | | | |
| Fast-RCNN [21] | 163 : | 29.2 | 5.5 | 24.4 | 0 | 208 : | 29.7 | 8.3 | 26.1 | 8.5 | | | | | |
| | 83 : | 15.6 | 1.8 | 9.7 | 0 | 104 : | 14.1 | 1.7 | 19.2 | 3.4 | | | | | |
| Our | 9 : | 57.9 | 62.4 | 32.7 | 48.6 | 46 : | 24.6 | 35.8 | 23.0 | 35.7 | | | | | |

#box indicates the number of **part** annotations for model learning, and the performance is evaluated by the values of (APP / AER). With the help of massive web images, our method only required 3%–95% number of the part annotations that were used by *SSDPM*, and achieved comparable performance to *SSDPM*.

tively⁷.

Then, we used the technique of [29] as the fourth baseline, namely *PLDPM*, which required annotations of both the parts and object poses for training. To enable a fair comparison, we only collected and labeled training samples that corresponded to the poses in our AoG.

The fifth baseline was another part model proposed by [7], namely *P-Graph*, which organized object parts into a graph and trained a SVM based on the part appearance features and inter-part relationships for part localization.

The sixth baseline was image matching, namely *Matching*, introduced in [44]. Unlike conventional matching be-

⁷Due to the limited number of training samples, the *bulldozer* and *horse* categories could produce at most four pairs of pose models for *SSDPM-5*. Training samples used in the baselines will be published after the paper acceptance.

tween automatically detected feature points [10, 28, 5], *Matching* used a graph template to match semantic parts of objects in images. For a fair comparison, *Matching* constructed a graph template for each pose in our AoG (*i.e.* using the template of the initial sample labeled in Storyline 4).

Then, we used the benchmark method for object detection, *i.e.* *Fast-RCNN* [21], as the seventh baseline to detect object parts. We chose the widely used 16-layer VGG network (VGG-16) [37] that was pre-trained based on the ImageNet dataset [12]. For each semantic part, we used [21] to fine-tuned the VGG-16 using the part annotations and obtained a specific part detector.

The eighth baseline was a method for interactive annotating and learning object parts, which was proposed in [4].

We called it *Interactive-DPM*. The idea of online interactive learning of object parts is quite close to our method.

Evaluation metrics: We used two ways to evaluate part localization performance. The first metric is the APP [19] (Average Percentage of Parts that are correctly estimated). Given each true object, we used the best pose component in the model (with the highest score) to explain the object. Then, for each object part of the pose, we used the “ $IOU > 50\%$ ” criterion [31, 2] to identify correct part localizations. We computed such a percentage for each type of semantic parts, and APP is the average for all the part types. To reduce the effects of object detection on the APP, we detect the object within the image region of $[c_w \pm w]$ and $[c_h \pm h]$, where $w/h/(c_w, c_h)$ indicates the width/height/center of the true object bounding box.

The second evaluate metric is the AER (average explanation rate) of objects. When an object is detected⁸, if more than 2/3 of the parts in its pose component are correctly localized, we consider this object being correctly explained by this component. Fig. 7 compares part localization performance between different baselines given a certain annotation cost. Different curves/dots correspond to different baselines. For most baselines, the annotation cost is the number of labeled parts on training samples. However, for our QA system, the overall cost consists of the cost of labeling parts and that of making yes/no judgements. Therefore, we drew two curves for our method: *Ours* simply used the number of part boxes as the cost, whereas *Ours (full cost)* computed the cost as $(\#ofboxes) + 0.2 \times (\#ofjudgements)$ (a judgment costs about 1/5 of the time of labeling a part).

Note that the baseline of *Interactive-DPM* [4] cannot detect bounding boxes for object parts, but localizes the center of each part. Therefore, just as in [47], we used the “average localization error” to evaluate the part localization accuracy. We normalized pixel error with respect to the part size, computed as $\sqrt{part\ height^2 + part\ width^2}$. In Fig. 8, we compared the proposed method with *Interactive-DPM* [4] in terms of the average localization error.

Comparison of learning efficiency. We used the ten category models in the *AoG-10* to explain its corresponding objects. For each category, 75 images were prepared as testing images to compute the object explanation rate. Fig. 5 illustrates part localization performance of the *AoG-10*. Fig. 7 shows the average explanation rate over the ten categories. To evaluate our method, we computed the performance of intermediate models for each category, which were trained during the QA procedure with different number of storylines/questions. Given the same amount of labeling, our method exhibited about twice explanation rate of *Matching*. When our method only used 125 bounding boxes for training, i.e. 3% of *SSDPM-3*’s annotation cost

(4258 boxes), it still achieved higher explanation rate than *SSDPM-3* (22.4% vs. 17.9%).

Performance on the Pascal VOC2007: We learned the *AoG-7* from web images, and tested it using *horse*, *motor-bike*, *bus*, *aeroplane*, and *bicycle* images with the *left* and *right* poses. This subset of Pascal images have been widely used for weakly supervised learning [31, 11]. We compare our method with the baselines of *SSDPM*, *P-Graph*, *Fast-RCNN*, and *Interactive-DPM*. *SSDPM* used the Pascal training samples with the *left* and *right* poses for learning. We required *SSDPM* to produce the maximum number of components for each category. Table 2 shows the result. *SSDPM* models were learned from different numbers of part annotations. In Fig. 8, we compared the average localization errors of *Interactive-DPM* [4] and our method.

Unlike *SSDPM*, *P-Graph* and *Interactive-DPM* directly learning part knowledge from a few annotations, we localized semantic parts on a latent object structure that was mined from unannotated web images. Thus, our method suffered less from the over-fitting problem. In addition, although *Fast-RCNN* has exhibited superior performance in most object detection tasks, it did not perform that well in part detections. It is because 1) object parts were usually small in images, and without contextual knowledge, the low-resolution part patches could not provide enough distinguishing information; and 2) that we only annotated a small number of samples for each part (e.g. $49/4 = 12.25$ annotations for each part of the aeroplane), which was not enough to learn a solid *Fast-RCNN* model. In contrast, our method did not require a large number of annotations for learning/fine-tuning, and modeled the spatial relationships between parts. Therefore, in Table 2 and Fig. 8, our method used less part annotations but achieved better localization accuracy.

5. Discussion and conclusions

In this study, we used human-computer dialogues to mine a nine-layer hierarchy of visual concepts from web images and build an *AoG*. Unlike the conventional problem of object detection that only focuses on object bounding boxes, our *AoG* localized semantic parts of objects and simultaneously aligned common shape primitives within each part, in order to provide a deep understanding of object statuses. In addition, our method combined active question answering and weakly supervised web-scale learning, which exhibited high efficiency at knowledge mining in experiments.

In recently years, the development of the CNN has made great progress in object detection. Thus, it becomes more and more important to go beyond the object level and pursue the transparent understanding of deep object structures. Unlike object parts, the accuracy of detailed sketches within each local part is difficult to evaluate, many of the sketches represent latent semantics within object parts.

⁸To simplify the evaluation metric, we only detected the best object from an image and ignored the others.

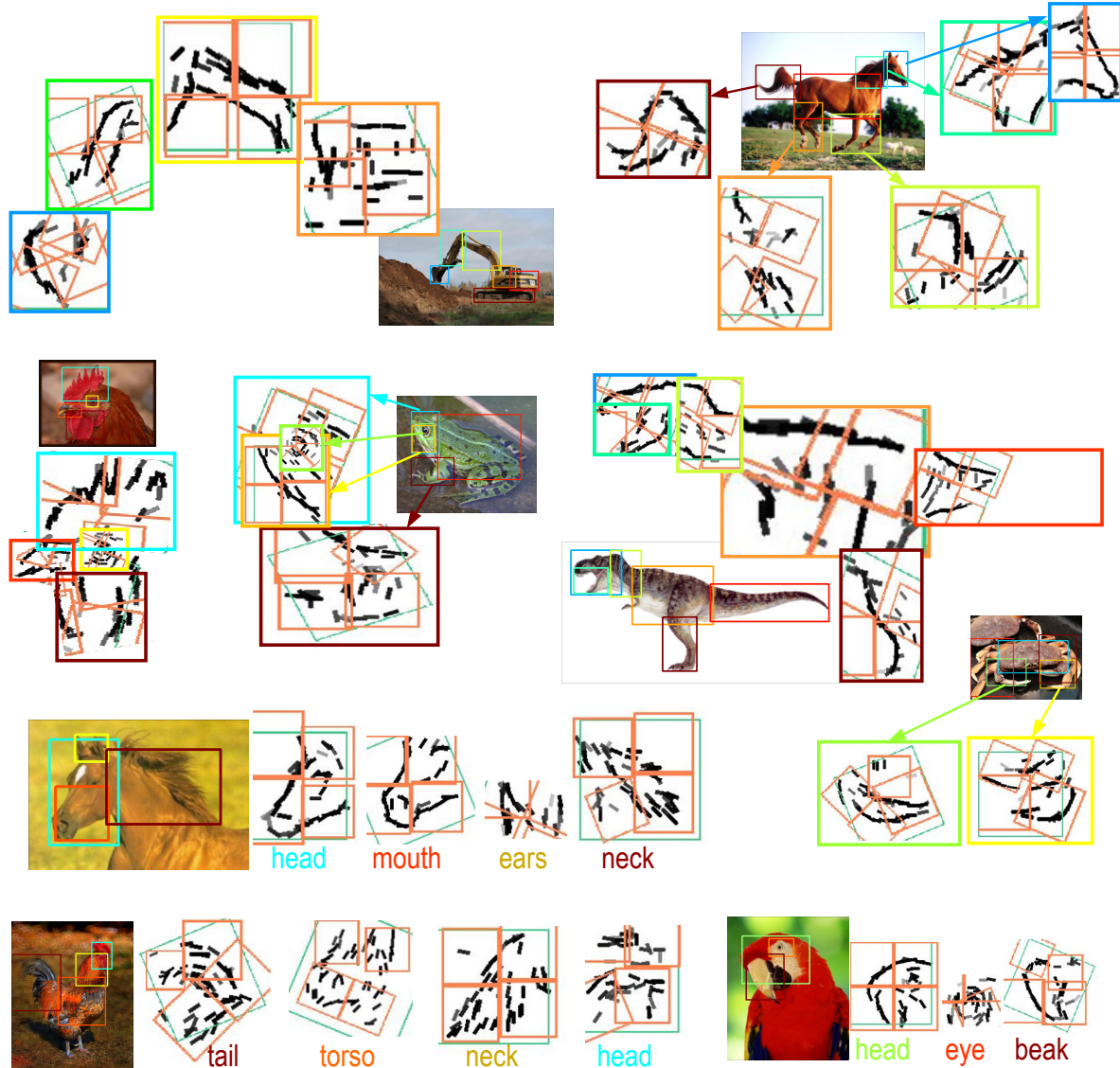


Figure 6. Deep semantics within object parts. We mine the common structure within each object part, and represent the shape primitives in Layers 5–9 of the AoG. In fact, some of these shape primitives have certain latent semantics, *e.g.* the mandible of a Tyrannosaurus rex within its “mouth” part. Given an images, the shape primitives can be aligned to their corresponding image regions with a certain deformation.

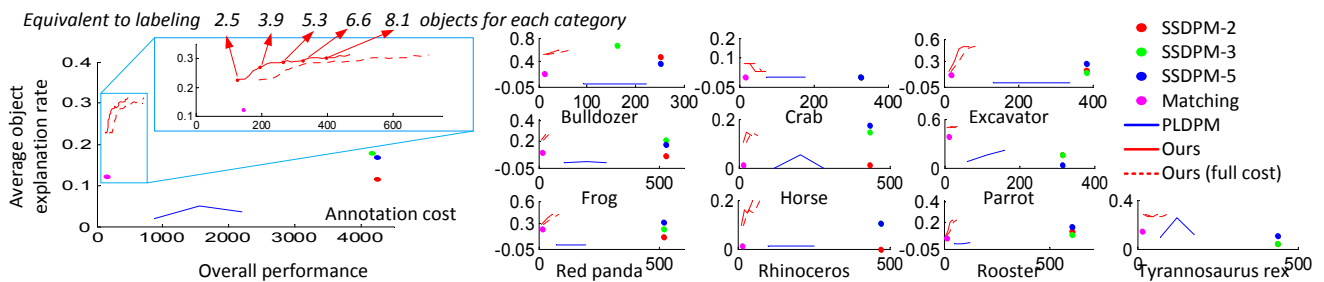


Figure 7. Comparisons in the efficiency of knowledge mining. The annotation cost (horizontal axis) is computed based on **part** annotations. The top line shows such annotations are equivalent to labeling how many **objects** for each category. Instead of preparing a large training set for supervised methods, our method can achieve multiple-shot learning (on average, 2–10 shots for each part, here).

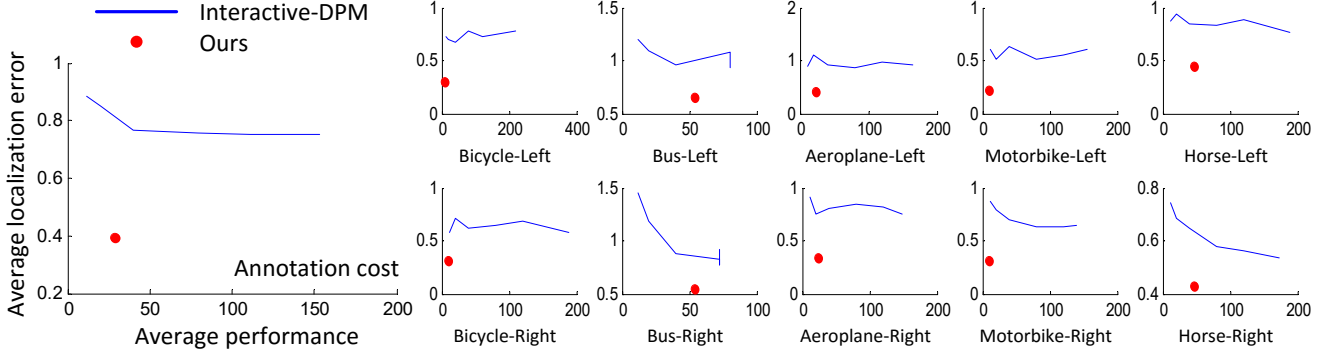


Figure 8. Comparisons with *Interactive-DPM* in terms of average localization errors. The annotation cost (horizontal axis) is computed based on **part** annotations. Our method exhibits low localization errors, given a limited number of part annotations.

Search engines usually return incorrect images without target objects and simple objects that are placed in image centers and well captured without occlusions. Thus, life-long learning studies, such as [6] and ours, mainly first learn from simple samples, and then gradually switch to difficult ones. In fact, comprehensive mining of all object poses, including infrequent poses, remains a challenging long-tail problem.

In this study, we aimed to explore a general QA system for model mining and test its efficiency. Thus, we applied simple features and trained simple classifiers for simplicity. However, we can extend the QA system to incorporate more sophisticated techniques (*e.g.* connecting the AoG to the CNN) to achieve better performance.

6. Appendix

6.1. Objective function of graph mining

The objective function in [44] was proposed in the form of

$$\operatorname{argmin}_{\theta_{PO_i}} \left\{ \sum_{P \in Ch(PO_i)} \mathcal{E}_P^+ - \sum_{P \in Ch(PO_i)} \mathcal{E}_P^- + \lambda \text{Complexity}(\theta_{PO_i}) \right\}$$

where the pattern complexity $\text{Complexity}(\theta_{PO_i})$ is formulated using the node number in the pattern, $\text{Complexity}(\theta_{PO_i}) = |Ch(PO_i)| + \beta \sum_{P \in Ch(PO_i)} |Ch(P)|$. Then, the terms of \mathcal{E}_P^+ and \mathcal{E}_P^- are the average responses of part node P among positive images and negative images, respectively:

$$\begin{aligned} \mathcal{E}_P^+ &= E_{I \in \hat{\mathbf{I}}_{PO_i}} \left\{ S_I(P) + \operatorname{mean}_{P' \in Ch(PO_i), P' \neq P} w_{PP'} S_I(P, P') \right\} \\ \mathcal{E}_P^- &= E_{I \notin \hat{\mathbf{I}}_{PO_i}} \left\{ S_I(P) + \operatorname{mean}_{P' \in Ch(PO_i), P' \neq P} w_{PP'} S_I(P, P') \right\} \end{aligned}$$

Considering $S_I^{app}(PO_i) = 0$, we can rewrite the objective as

$$\begin{aligned} & \operatorname{argmin}_{\theta_{PO_i}} \left\{ \sum_{P \in Ch(PO_i)} \mathcal{E}_P^+ - \sum_{P \in Ch(PO_i)} \mathcal{E}_P^- + \lambda \text{Complexity}(\theta_{PO_i}) \right\} \\ &= \operatorname{argmax}_{\theta_{PO_i}} \left\{ |Ch(PO_i)| \left\{ \frac{E}{I \notin \hat{\mathbf{I}}_{PO_i}} [S_I(PO_i)] - \frac{E}{I \in \hat{\mathbf{I}}_{PO_i}} [S_I(PO_i)] \right\} \right. \\ & \quad \left. - \lambda \text{Complexity}(\theta_{PO_i}) \right\} \\ &= \operatorname{argmax}_{\theta_{PO_i}} \left\{ E_{I \in \hat{\mathbf{I}}_{PO_i}} [S_I(PO_i)] - E_{I \notin \hat{\mathbf{I}}_{PO_i}} [S_I(PO_i)] \right. \\ & \quad \left. - \frac{\lambda \text{Complexity}(\theta_{PO_i})}{|Ch(PO_i)|} \right\} \end{aligned}$$

In addition, the average score of $S_I(PO_i)$ for negative (background) images is normalized to zero. Therefore, we can further approximate the objective as

$$\operatorname{argmax}_{\theta_{PO_i}} \left\{ E_{I \in \hat{\mathbf{I}}_{PO_i}} [S_I(PO_i)] - \frac{\lambda \text{Complexity}(\theta_{PO_i})}{|Ch(PO_i)|} \right\}$$

Therefore, if we redefine a new complexity $\text{Complexity}^{new}(\theta_{PO_i}) = \text{Complexity}(\theta_{PO_i}) / |Ch(PO_i)|$, we can write the objective function as

$$\operatorname{argmax}_{\theta_{PO_i}} \left\{ E_{I \in \hat{\mathbf{I}}_{PO_i}} [S_I(PO_i)] - \lambda \text{Complexity}^{new}(\theta_{PO_i}) \right\}$$

References

- [1] S. Antol, A. Agrawal, J. Lu, M. Mitchell, D. Batra, C. L. Zitnick, and D. Parikh. Vqa: Visual question answering. *In ICCV*, 2015. 2
- [2] H. Azizpour and I. Laptev. Object detection using strongly-supervised deformable part models. *In ECCV*, 2012. 3, 8, 9, 10
- [3] J. L. Ba, K. Swersky, S. Fidler, and R. Salakhutdinov. Predicting deep zero-shot convolutional neural networks using textual descriptions. *In ICCV*, 2015. 2
- [4] S. Branson, P. Perona, and S. Belongie. Strong supervision from weak annotation: Interactive training of deformable part models. *In ICCV*, 2011. 2, 3, 9, 10

- [5] T. S. Caetano, J. J. McAuley, L. Cheng, Q. V. Le, and A. J. Smola. Learning graph matching. *In PAMI*, 2009. 9
- [6] X. Chen and A. Gupta. Webly supervised learning of convolutional networks. *In ICCV*, 2015. 2, 12
- [7] X. Chen, R. Mottaghi, X. Liu, S. Fidler, R. Urtasun, and A. Yuille. Detect what you can: Detecting and representing objects using holistic models and body parts. *In CVPR*, 2014. 3, 9
- [8] X. Chen, A. Shrivastava, and A. Gupta. Neil: Extracting visual knowledge from web data. *In ICCV*, 2013. 2
- [9] X. Chen, A. Shrivastava, and A. Gupta. Enriching visual knowledge bases via object discovery and segmentation. *In CVPR*, 2014. 2
- [10] M. Cho, K. Alahari, and J. Ponce. Learning graphs to match. *In ICCV*, 2013. 9
- [11] M. Cho, S. Kwak, C. Schmid, and J. Ponce. Unsupervised object discovery and localization in the wild: Part-based matching with bottom-up region proposals. *In CVPR*, 2015. 2, 10
- [12] J. Deng, W. Dong, R. Socher, L.-J. Li, K. Li, and L. Fei-Fei. Imagenet: A large-scale hierarchical image database. *In CVPR*, 2009. 9
- [13] J. Deng, J. Krause, A. C. Berg, A. Berg, and L. Fei-Fei. Hedging your bets: Optimizing accuracy-specificity trade-offs in large scale visual recognition. *In CVPR*, 2012. 2
- [14] J. Deng, O. Russakovsky, J. Krause, M. Bernstein, A. Berg, and L. Fei-Fei. Scalable multi-label annotation. *In CHI*, 2014. 2
- [15] T. Deselaers, B. Alexe, and V. Ferrari. Localizing objects while learning their appearance. *In ECCV*, 2010. 2
- [16] C. Doersch, A. Gupta, and A. A. Efros. Unsupervised visual representation learning by context prediction. *In ICCV*, 2015. 2
- [17] T. Durand, N. Thome, and M. Cord. Mantra: Minimum maximum latent structural svm for image classification and ranking. *In ICCV*, 2015. 3
- [18] M. Everingham, L. Gool, C. Williams, J. Winn, and A. Zisserman. *The PASCAL Visual Object Classes Challenge 2007 (VOC2007) Results*. 8
- [19] V. Ferrari, M. Marin-Jimenez, and A. Zisserman. Progressive search space reduction for human pose estimation. *In CVPR*, 2008. 10
- [20] S. Gavves, T. Mensink, T. Tommasi, C. Snoek, and T. Tuytelaars. Active learning revisited: Reusing past datasets for future tasks. *In ICCV*, 2015. 2
- [21] R. Girshick. Fast r-cnn. *In ICCV*, 2015. 9
- [22] G. Gkioxari, R. Girshick, and J. Malik. Actions and attributes from wholes and parts. *In ICCV*, 2015. 3
- [23] G. Kim and E. P. Xing. On multiple foreground cosegmentation. *In CVPR*, 2012. 2
- [24] V. Kolmogorov. Convergent tree-reweighted message passing for energy minimization. *In PAMI*, 28(10):1568–1583, 2006. 5
- [25] C. Kong, D. Lin, M. Bansal, R. Urtasun, and S. Fidler. What are you talking about? text-to-image coreference. *In CVPR*, 2014. 2
- [26] K. Konyushkova, R. Sznitman, and P. Fua. Introducing geometry in active learning for image segmentation. *In ICCV*, 2015. 2
- [27] A. Krizhevsky, I. Sutskever, and G. Hinton. Imagenet classification with deep convolutional neural networks. *In NIPS*, 2012. 2
- [28] M. Leordeanu, R. Sukthankar, and M. Hebert. Unsupervised learning for graph matching. *In IJCV*, 2012. 9
- [29] B. Li, W. Hu, T. Wu, and S.-C. Zhu. Modeling occlusion by discriminative and-or structures. *In ICCV*, 2013. 9
- [30] C. Long and G. Hua. Multi-class multi-annotator active learning with robust gaussian process for visual recognition. *In ICCV*, 2015. 2
- [31] M. Pandey and S. Lazebnik. Scene recognition and weakly supervised object localization with deformable part-based models. *In ICCV*, 2011. 2, 10
- [32] Z. Ren, C. Wang, and A. Yuille. Scene-domain active part models for object representation. *In ICCV*, 2015. 3
- [33] O. Russakovsky, L.-J. Li, and L. Fei-Fei. Best of both worlds: human-machine collaboration for object annotation. *In CVPR*, 2015. 2
- [34] Z. Si and S.-C. Zhu. Learning hybrid image templates (hit) by information projection. *In PAMI*, 2012. 4
- [35] Z. Si and S.-C. Zhu. Learning and-or templates for object recognition and detection. *In PAMI*, 2013. 2, 4, 5, 7
- [36] M. Simon and E. Rodner. Neural activation constellations: Unsupervised part model discovery with convolutional networks. *In ICCV*, 2015. 2, 3
- [37] K. Simonyan and A. Zisserman. Very deep convolutional networks for large-scale image recognition. *In ICLR*, 2015. 9
- [38] H. O. Song, R. Girshick, S. Jegelka, J. Mairal, Z. Harchaoui, and T. Darrell. On learning to localize objects with minimal supervision. *In ICML*, 2014. 2
- [39] C. Sun, C. Gan, and R. Nevatia. Automatic concept discovery from parallel text and visual corpora. *In ICCV*, 2015. 2
- [40] Q. Sun, A. Laddha, and D. Batra. Active learning for structured probabilistic models with histogram approximation. *In CVPR*, 2015. 2
- [41] K. Tu, M. Meng, M. W. Lee, T. E. Choe, and S.-C. Zhu. Joint video and text parsing for understanding events and answering queries. *In IEEE MultiMedia*, 2014. 2
- [42] S. Vijayanarasimhan and K. Grauman. Large-scale live active learning: Training object detectors with crawled data and crowds. *In CVPR*, 2011. 2
- [43] X. Wang, Z. Zhu, C. Yao, and X. Bai. Relaxed multiple-instance svm with application to object discovery. *In ICCV*, 2015. 2
- [44] Q. Zhang, Y.-N. Wu, and S.-C. Zhu. Mining and-or graphs for graph matching and object discovery. *In ICCV*, 2015. 2, 4, 5, 7, 8, 9, 12
- [45] J.-Y. Zhu, J. Wu, Y. Xu, E. Chang, and Z. Tu. Unsupervised object class discovery via saliency-guided multiple class learning. *In PAMI*, 2014. 2
- [46] M. Zhu, X. Zhou, and K. Danilidiis. Single image pop-up from discriminatively learned parts. *In ICCV*, 2015. 3

- [47] X. Zhu and D. Ramanan. Face detection, pose estimation, and landmark localization in the wild. *In CVPR*, 2012. 10
- [48] Y. Zhu, R. Kiros, R. Zemel, R. Salakhutdinov, R. Urtasun, A. Torralba, and S. Fidler. Aligning books and movies: Towards story-like visual explanations by watching movies and reading books. *In ICCV*, 2015. 2